scientific reports

Check for updates

OPEN

Exosomal miR-92a-3p serves as a promising marker and potential therapeutic target for adenomyosis

Wanqi Shao[1,6], Yayuan Yu[2,6], Jianzhang Wang[3,6], Zhiruo Qiu[4], Shuyan Mei[4], Tao Cheng[4], Yichen Chen[5], Weili Zhu[2], Xiuhui Li[2]✉ & Xuan Che[2,4]✉

This study aimed to elucidate the role of microRNA-92a-3p (miR-92a-3p) in the pathogenesis of adenomyosis. We examined how miR-92a-3p, found in exosomes derived from ectopic lesions, influences the behaviour of endometrial cells, dorsal root ganglion (DRG), and human umbilical vein endothelial cells (HUVECs) and explored its potential as a non-invasive biomarker. Our findings revealed that miR-92a-3p was significantly upregulated in exosomes derived from ectopic adenomyotic lesions. This upregulation correlated with enhanced migration and invasion of eutopic endometrial cells, DRG, and HUVECs. Furthermore, this study demonstrated a significant correlation between miR-92a-3p levels in urinary exosomes and the clinical symptoms of adenomyosis, suggesting its potential as a non-invasive biomarker for the disease. This study elucidated an exosomal signalling process involving miR-92a-3p that drives pathological infiltration and angiogenesis to promote adenomyosis progression. Our findings highlight upregulated miR-92a-3p in biofluid exosomes as a promising non-invasive biomarker for diagnosing and monitoring adenomyosis and unveil novel targets and strategies for improved clinical management.

Keywords miR-92a-3p, Adenomyosis, Exosomes, Biomarker

Adenomyosis is a complex gynaecological condition characterised by the infiltration of endometrial tissue into the uterine muscle, resulting in significant morbidity among women[1,2].Despite advances in understanding its hormonal and genetic underpinnings, the molecular mechanisms, particularly the role of exosomal microRNAs (miRNAs), remain inadequately explored[3–5]. Therefore, identifying clinical biomarkers to aid in the diagnosis of adenomyosis is crucial[6,7].

MicroRNA-92a-3p (MiR-92a-3p) has been implicated in several cancers. Recent studies have highlighted the significance of miRNAs in various diseases. For instance, Mao et al. demonstrated that miR-92a-3p promotes the proliferation and invasion of gastric cancer by targeting KLF2[8]. Similarly, Huang found that miR-92a-3p enhances breast cancer cell proliferation and metastasis[9].These studies highlight the diverse roles of miR-92a-3p in oncology. Additionally, Ashok et al. identified miR-92a-3p as a potential blood-based biomarker for osteoblastic metastases in prostate adenocarcinoma[10], while Li and Luo showed that miR-92a-3p suppresses cell proliferation in Wilms' tumour[11]. These findings underscore the multifaceted roles of miRNAs in different pathological contexts. However, the specific role of miR-92a-3p in adenomyosis is not well defined[12].

There remains a significant gap in understanding the specific mechanisms by which miR-92a-3p influences adenomyosis,impeding the development of targeted therapeutic strategies and precise diagnostic tools for this debilitating condition.To bridge this gap, our study employed a comprehensive approach, including exosome purification[13],miRNA sequencing, and quantitative real-time polymerase chain reaction (qRT-PCR), to analyse the expression and role of miR-92a-3p in adenomyosis. We focused on its effects on various cell types, including endometrial cells, dorsal root ganglion (DRG), and human umbilical vein endothelial cells (HUVECs), and its potential as a non-invasive biomarker by correlating its levels in urinary exosomes with clinical symptoms. This study aims to provide a deeper understanding of miR-92a-3p's role in adenomyosis and contribute to improved diagnostic and therapeutic approaches.

[1]Jiaxing University Master Degree Cultivation Base, Zhejiang Chinese Medical University, Jiaxing 314000, China. [2]Department of Obstetrics and Gynecology, Jiaxing University Affiliated Maternity and Child Hospital, Jiaxing 314000, China. [3]Women's Hospital, School of Medicine, Zhejiang University, Hangzhou 310000, China. [4]Wenzhou Medical University, Wenzhou 325000, China. [5]Ningbo Institute of Medical Science, Ningbo 315000, China. [6]Wanqi Shao, Yayuan Yu and Jianzhang Wang contributed equally to this work. ✉email: lixiuxiusun@163.com; chexuan@zjxu.edu.cn

Materials and methods

Ethic approval

This investigation received ethical approval from the Ethics Committee of Jiaxing Maternal and Child Health Hospital (No. 2022-020). All methods were carried out in accordance with relevant guidelines and regulations, and explicit informed consent was obtained from all participants.

Patient plasma, urine, eutopic endometrium, and ectopic lesions of adenomyosis (ELA)

From early 2019 to the end of 2022, we systematically collected a diverse array of samples,including plasma, urine, eutopic endometrium, and ELA, at the hospital. The adenomyosis cohort comprised patients diagnosed through laparoscopy and subsequently confirmed by histopathology. Controls were patients who had undergone total hysterectomy for uterine leiomyomas, also confirmed by histopathological confirmation. Inclusion criteria were premenopausal women aged 35–50 years with adenomyosis and uterine fibroids who had undergone hysterectomy because of severe symptoms, lack of desire for fertility or failure of medical treatment, no use of any form of hormone therapy within at least 3 months, no smoking, and no history of other inflammatory diseases requiring surgical treatment. Exclusion criteria were incomplete clinical and pathological, co-existing malignant tumours, use of hormone replacement therapy, menopausal or pregnant women, hormone-dependent diseases such as endometriosis, and use of a hormone coil.

Throughout the sampling process, comprehensive clinical data were meticulously documented for each participant, including age, reproductive history, ultrasound-derived uterine diameter and volume,menstrual cycle characteristics,evaluation of menstrual flow based on the pictorial blood loss assessment chart, height, weight, body mass index, preoperative CA125 levels, hemoglobin concentration, platelet count, and dysmenorrhoea severity based on the visual analogue scale scoring method. We collected plasma samples into separation tubes, then centrifuged them at 3000×*g* for $15\,\mathrm{min}$ in a refrigerated centrifuge at $4\,^{\circ}\mathrm{C}$ and stored them at $-80\,^{\circ}\mathrm{C}$ for further analysis. We collected urine samples into $50\,\mathrm{mL}$ centrifuge tubes, then centrifuged at 2000×*g* for $20\,\mathrm{min}$ at room temperature and stored at $-80\,^{\circ}\mathrm{C}$ for further analysis.

Exosomes isolation

We used type III collagenase to digest the ectopic lesion tissue, which had been cut into small pieces. After the digestion, the supernatant was filtered to obtain an ectopic lesion tissue suspension. Exosomes from plasma, urine, ectopic lesion tissue suspension, and ectopic lesion cell supernatant were prepared by differential ultracentrifugation as described previously[14]. The plasma, urine, ELA, and their cellular supernatant were centrifuged at 500×*g* for $10\,\mathrm{min}$ at $4\,^{\circ}\mathrm{C}$. The supernatant was centrifuged at 2000×*g* for $10\,\mathrm{min}$ at $4\,^{\circ}\mathrm{C}$. The subsequent supernatant was then subjected to another centrifugation step at 1000×*g* for $30\,\mathrm{min}$ at $4\,^{\circ}\mathrm{C}$ and finally ultracentrifuged at 100,000×*g* for $90\,\mathrm{min}$ at $4\,^{\circ}\mathrm{C}$. Pellets containing total exosomes were resuspended in $0.5\,\mathrm{mL}$ of phosphate-buffered saline (PBS).

Cell culture

HUVECs were purchased from the China Centre for Type Culture Collection (Wuhan, China) and used for cell experiments between passages 2 and 3. Rat dorsal root ganglion cells (F11), serving as a neuronal model, were obtained from the European Collection of Authenticated Cell Cultures (United Kingdom). Cells were cultured in Dulbecco's Modified Eagle Medium (DMEM)/F11 medium/HUVECs medium supplemented with 10% foetal bovine serum (FBS) (Biological Industries, Israel) and kept in a humidified 5% CO_2 atmosphere at $37\,^{\circ}\mathrm{C}$. Experiments were performed when the cells reached 70-80% confluence.

Isolation of primary cells from eutopic endometrium and ectopic lesions

Human endometrial tissue and ectopic lesions were collected from patients with and without adenomyosis. Samples were washed with $1\times$ PBS and cut into $1\,\mathrm{mm}^3$ pieces, then digested with type III collagenase in an orbital shaker at $37\,^{\circ}\mathrm{C}$ for $60\,\mathrm{min}$. Digestion was halted by adding an equal volume of complete culture medium. The mixture was aspirated and dispensed for $5\,\mathrm{min}$, then filtered through 100 μm sieves to remove debris. This was followed by the use of a $40\mu\mathrm{m}$ sieve to separate epithelial and stromal cells. The obtained cells were resuspended in DMEM/F11 medium containing 10% FBS in a humidified incubator at $37\,^{\circ}\mathrm{C}$ and 5% CO_2 . Cultures of ectopic endometrial cells were utilized during their second to third passages.

Transmission electron microscopy (TEM)

Ten microlitres of exosome solution were applied to a copper mesh, incubated at room temperature for $10\,\mathrm{min}$, and washed with sterile distilled water. Thereafter, the excess liquid was removed with absorbent paper. Negative staining was performed by adding 10 μL of 2% uranyl acetate to the copper mesh for $1\,\mathrm{min}$. The excess liquid was removed by suction on a filter paper and dried under an incandescent lamp for $2\,\mathrm{min}$. Samples were examined by TEM (JEOL, Tokyo, Japan).

Nanoparticle tracking analysis (NTA)

A laser light source was used to illuminate the nanoparticle suspension, and the scattered light from the nanoparticles was detected to determine concentration. The ZetaView PMX 110 particle matrix was used to determine the concentration of isolated exosomes under $405\,\mathrm{nm}$ emission light. Exosomes were diluted with PBS to concentrations ranging from 1×10^7 particles/ml to 1×10^9 particles/ml, and their size and mass were measured. Additionally, the particle motion trajectory of exosomes was analyzed.

Western blot analysis

We detected the exosomal markers CD9, CD63, and TSG101 through western blot analysis. Proteins from the exosomes were isolated with radioimmunoprecipitation assay lysis buffer (Beyotime, Shanghai, China). These lysates underwent a $10\,\mathrm{min}$ incubation at $0\,^{\circ}\mathrm{C}$ before the supernatants were spun down at $10000 \times g$ for $20\,\mathrm{min}$ at $4\,^{\circ}\mathrm{C}$. Protein concentration was determined using the bicinchoninic acid protein assay (Beyotime, Shanghai, China). Based on the quantitative results, we calculated the amount of sample (10–30 μg) to be loaded onto exosomes. We added 5X sodium dodecyl sulfate buffer in proportion, vortexed and mixed thoroughly, then denatured at $95\,^{\circ}\mathrm{C}$ for $5\,\mathrm{min}$ for protein electrophoresis. After electrophoresis, we removed the separating gel and transferred the target protein bands (exosome positive protein markers CD9/TSG101/CD63 and negative protein marker Calnexin -three positives and one negative) from the gel to a polyvinylidene fluoride membrane by electrotransfer. After blocking with 3% bovine serum albumin blocking solution, we incubated with primary and secondary antibodies, then used enhanced chemiluminescence bioluminescence reagent for imaging in the image acquisition instrument. The bands were analysed using Quantity One image analysis software.

Exosomal RNA extraction and microarray analysis of miRNA expression

Exosomal miRNAs were extracted using TRIzol reagent (Ambion Life Technologies), following the manufacturer's guidelines. The quality and distribution of the miRNAs were assessed using the Agilent 2100 Bioanalyzer. MiRNA expression profiling was undertaken using the Agilent Human miR v21.0 array, which encompasses 2,549 mature human miRNAs. Following hybridization, the chip underwent scanning with the G2565BA Microarray Scanner (Agilent Technologies) and subsequent analysis using GenePix Pro software v4.1 (Molecular Devices Corporation, San Jose, CA). Differential expression of miRNAs was determined through paired t-test analysis, employing a significance threshold of $P < 0.05$ and fold change criteria of ≤ 0.5 or ≥ 2.

qRT-PCR

Total RNAs were isolated using TRIzol reagent (Ambion Life Technologies) according to the manufacturer's instructions. A mirVana^{TM} miRNA isolation kit was used to extract miRNAs from the plasma exosome samples according to the manufacturer's protocol (Thermo Fisher Scientific, MA, USA). For the quantification of miRNA expression levels, RT-PCR reactions were performed using the TianGen miRNA reverse transcription kit (TianGen Biochemical Technology, China) and TianGen Universal PCR Master Mix, according to the manufacturer's protocols. All reactions were performed in triplicate, and let-7d-5p miRNA served as the internal control. Results were analysed using the 2-Δ ΔCt method.

Exosomes co-cultured with endometrial epithelial cells (EEC), endometrial stromal cells (ESC), F11, and HUVECs

Exosomes derived from ELA (ELA-exo) were labelled using PKH67 fluorescent cell linker kits (MeRCK mini67, United States) following the manufacturer's protocol. In brief, 20 μL of exosomes were diluted with $1\,\mathrm{mL}$ of diluent C and 6 μL of PKH67 dye. The labelled exosomes were washed in PBS for $2\,\mathrm{h}$ at 190,000×9. Finally, EEC, ESC, F11, and HUVECs were incubated with PKH67-labelled exosomes for $6\,\mathrm{h}$ at $37\,^{\circ}\mathrm{C}$. The uptake of exosomes by EEC, ESC, F11, and HUVECs was observed using a confocal laser microscope (Olympus FV3000, Tokyo, and Japan).

Cell transfection

MiR-92a-2p mimics, miR-92a-2p mimics negative control (mimics NC), miR-92a-2p inhibitor, miR-92a-2p inhibitor negative control (inhibitor NC) (Gene Pharma, Germany) were designed, synthesised, and transfected into EEC, ESC, F11, HUVECs according to the manufacturer's protocol.

Cell proliferation assay

The proliferation of F11 and HUVECs was measured using the Cell Counting Kit-8 (CCK-8; UElandy Inc, China) according to the manufacturer's protocols. F11 and HUVECs were seeded into 96-well plates. At time intervals of 0, 24, 48, and 72 h, 10 μL of CCK-8 reagent was introduced into each well, followed by a $4\,\mathrm{h}$ incubation at $37\,^{\circ}\mathrm{C}$. Post incubation, absorbance was recorded at $450\,\mathrm{nm}$ using a microplate spectrophotometre (Thermo Fisher Scientific, USA).

Cell migration and invasion assay

Transwell chambers were precoated with 300 μg/mL Matrigel (BD Biosciences, USA). EEC, EPC, F11, and HUVECs in DMEM/F11 medium/HUVEC medium were added to the upper chamber of a Transwell insert. The lower chamber was filled with medium enriched with 20% FBS. After $24\,\mathrm{h}$ of incubation at $37\,^{\circ}\mathrm{C}$, non-invading cells were removed. Cells invading the lower chamber of the Transwell insert were fixed with paraformaldehyde and stained with 0.1% crystal violet. Cell invasion was analyzed by counting invading cells in five randomly selected fields under a 20X microscope. The mean and standard deviation were calculated, and a t-test was performed to assess differences in migration or invasion under different conditions. Cell migration assays were conducted using an identical approach, excluding the use of Matrigel.

Tube formation assay

Matrigel was thawed overnight at $4\,^{\circ}\mathrm{C}$ and then applied to a 96-well plate, which was incubated at $37\,^{\circ}\mathrm{C}$ for $60\,\mathrm{min}$. HUVECs, following transfection at a density of 1×10^4 cells per well, were plated in 96-well plates and incubated for $4\,\mathrm{h}$ at $37\,^{\circ}\mathrm{C}$ in a humidified incubator with 5% CO_2. Tube formation was observed, and images were captured using a light microscope. The number of branch points per well was analysed and quantified using ImageJ software.

Statistical analysis

Statistical analysis was performed using GraphPad Prism 6.0 (GraphPad Software, San Diego, California, USA) and SPSS19.0 (IBM Company, California, USA). Statistically significant differences between patients with adenomyosis and negative controls were identified using the two-tailed Student's t-test or Mann-Whitney U test. Mean ± standard error of the mean was depicted by error bars. To assess the diagnostic significance of the urinary exosomal miRNAs, the area under the curve (AUC) of the receiver operating characteristic (ROC) curve was calculated. Statistical significance was set at $P < 0.05$.

Results

Exosome purification and characterization

Morphological studies of plasma-, tissue-, and urine-derived exosomes from patients with adenomyosis were performed by TEM. TEM images revealed typical exosome structures (Fig. 1A–C). NTA demonstrated that the diameter distribution of exosomes ranged from approximately 30 nm to 150 nm (Fig. 1D–F). Western blot analysis was used to identify the exosome markers CD63, CD9, and TSG101. Calnexin, an intracellular protein, was found to be negatively expressed (Fig. 1G,H and S1).

Mir-92a-3p is highly expressed in exosomes derived from adenomyosis patient plasma and adenomyosis lesion tissue, especially in adenomyosis lesion tissue sources

Exosomes regulate numerous physiological activities through exosomal miRNA. Therefore, we explored the miRNAs in plasma exosomes that may play a role in adenomyosis. First, miRNA deep sequence analysis was performed to identify significantly different miRNAs between adenomyosis and controls (eight patients with adenomyosis and eight non-adenomyosis controls). A total of 82 differentially expressed exosome miRNAs were

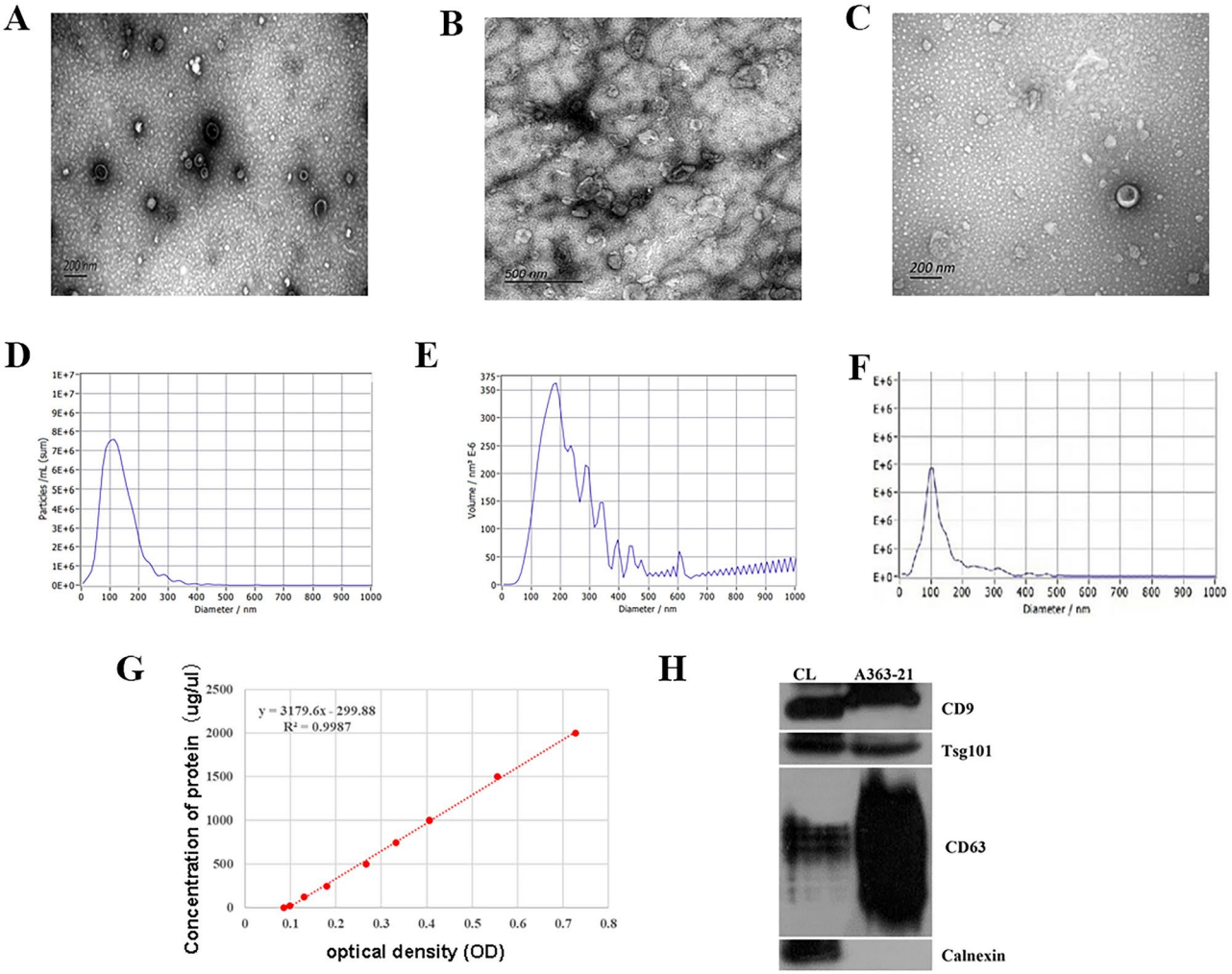

Figure 1. Identification of isolated exosomes. Transmission electron microscoc for plasma (**A**), tissue(**B**) and urine (**C**) exosomes. (**E** and **F**) NanoSight analysis for plasma (**D**), tissue (**E**) and urine (**F**) exosomes. (**G**) Protein content of plasma-derived exosomes. (**H**) CD9, CD63 and Tsg101 which are the protein markers of exosomes, were analyzed by Western blot analysis in the exosomes and exosome-free plasma. Calnexin were used as the loading.

screened. Compared with the control group, 22 miRNAs were upregulated and 24 miRNAs were downregulated in the adenomyosis group (Fig. 2A,B and Table S1). We selected the six most significantly upregulated miRNAs (miR-425-5p, miR-3615, miR-92a-3p, miR-382-5p, miR-423-3p, and miR-181-5p) for qRT-PCR verification. Our results showed that miR-92a-3p in plasma exosomes of patients with adenomyosis was significantly upregulated (Fig. 2C). Furthermore, we expanded the sample and measured miR-92a-3p in exosomes derived from plasma and ELA through qRT-PCR (45 patients with adenomyosis and 21 non-adenomyosis controls) (Fig. 2D,E). Surprisingly, miR-92a-3p in ELA-exo was more significantly upregulated than in plasma-derived exosomes compared to controls.

MiR-92a-3p in ELA-exo promotes the migration and infiltration of eutopic endometrial cells in adenomyosis

As we found that miR-92a-3p in ELA-exo was significantly upregulated, we further determined whether miR-92a-3p in exosomes derived from adenomyotic ectopic lesions played a crucial role in endometrial cells in adenomyosis(Fig. S2). EEC and ESC cells were incubated with ELA-exo, and exosomes were labelled with the green lipophilic fluorescent dye PKH67. After 6 h of incubation with PKH67-labeled exosomes, confocal images showed that the cells were positive for PKH67 fluorescence, suggesting that the exosomes were internalised by EEC and ESC (Fig. 3A).

Based on previous results, miR-92a-3p is a key miRNA enriched in exosomes derived from ectopic adenomyotic lesions. We examined the effects of miR-92a-3p on the migration and infiltration of endometrial cells. EEC and ESC were transfected with a mimic and an inhibitor of miR-92a-3p, and the efficiency of transfection was confirmed using real-time PCR (Fig. 3B). Transwell assays showed that miR-92a-3p promoted migration and invasion, and downregulation of miR-92a-3p inhibited the migration and invasion of adenomyotic eutopic endometrial cells (Fig. 3C,D). Overall, our results indicate that miR-92a-3p derived from ectopic adenomyotic lesions promotes the migration and invasion of adenomyotic eutopic endometrial cells, thus promoting the development of adenomyosis.

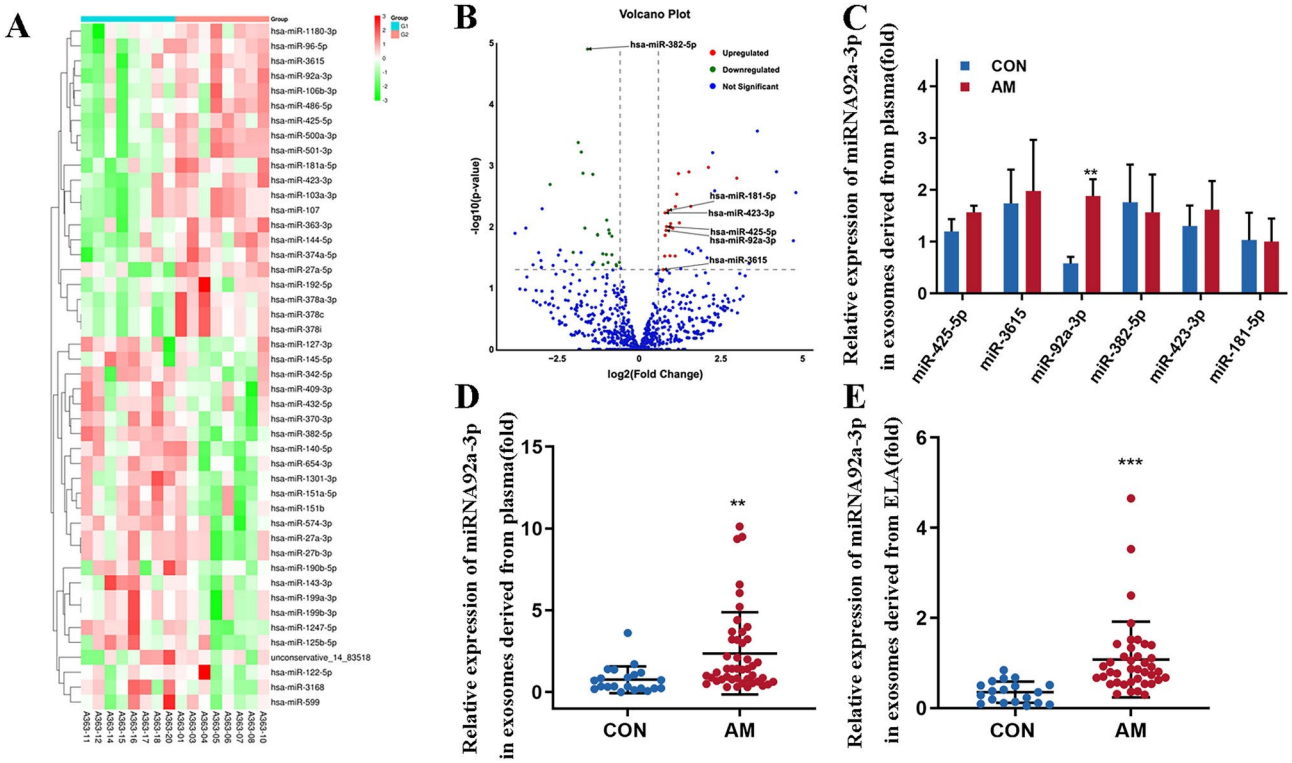

Figure 2. miRNA microarray profiling and qRT-PCR was used to explore the expression of exosomal miR-92a-3p in plasma and ectopic lesions of adenomyosis (ELA). Significant expression of 46 miRNAs with $P < 0.05$; red, 22 upregulated miRNAs; green, 24 downregulated miRNAs. Bonferroni correction for multiple comparisons. (**B**) Diagram showing 82 differentially expressed miRNAs; green, downregulated miRNAs; blue, not differentially expressed miRNA; red, upregulated miRNAs Bonferroni correction for multiple comparisons. (**C**) The differential miRNAs of plasma-derived exosomes were verified by qRT-PCR (normalized to let-7d-5p). (**D**) qRT-PCR was used to explore the expression of plasma exosomal miR-92a-3p in 45 patients with adenomyosis and 21 individuals in the control group(normalized to let-7d-5p). (**E**) qRT-PCR was used to explore the expression of ectopic lesions supernatant exosomal miR-92a-3p in 40 patients with adenomyosis and 19 individuals in the control group (normalized to let-7d-5p). The experiments were repeated three times. $^{*}P < 0.05$, $^{**}P < 0.01$, $^{***}P < 0.001$.

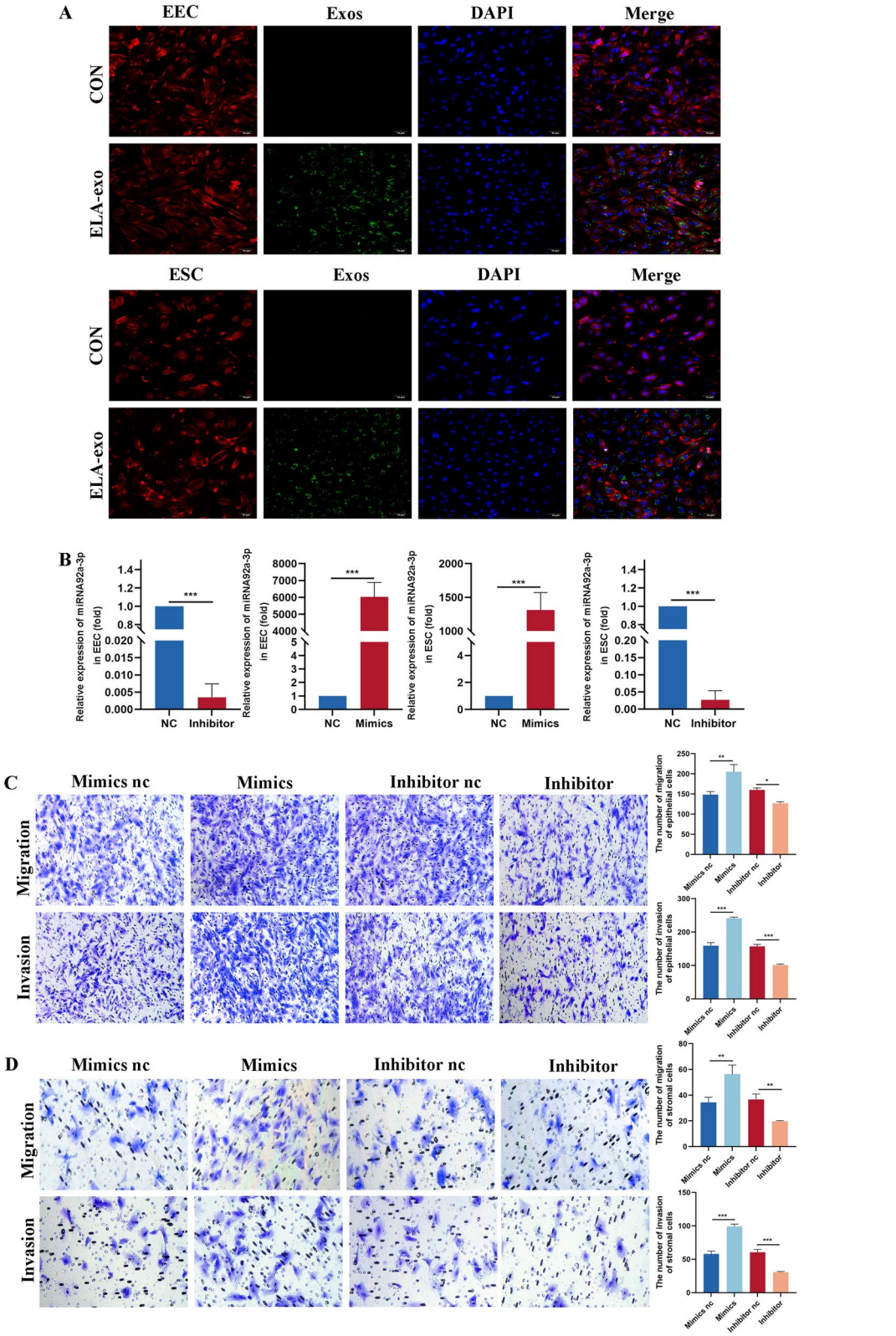

Figure 3. Effects of miR-92a-3p in exosomes derived from ectopic lesions of adenomyosis on the migration and infiltration of eutopic endometrial stromal cells (ESC) and endometrial epithelial cells (EEC). (**A**) Representative immunofluorescence images showing the internalization of PKH67-labeled ectopic endometrial cells-derived exosomes (green) by ESC, EEC stained with phalloidine (red). Cell nuclei were stained with DAPI (blue). Scale bars=50 mm. (**B**) qRT-PCR verified ESC and EEC transfection efficiency. (**C**) Representative images of transwell Matrigel invasion assay and migration assays in ESC pretreated with transfection. Scale bars=200 mm. (**D**) Representative images of transwell Matrigel invasion assay and migration assays in EEC pretreated with transfection. $^{*}P < 0.05$, $^{**}P < 0.01$ and $^{***}P < 0.001$.

MiR-92a-3p in ELA-exo promotes the proliferation, migration, and infiltration of DRG

We examined the effect of miR-92a-3p in exosomes derived from ectopic adenomyotic lesions on DRG. We also co-cultured F11 cells with the PKH67-labelled exosomes. The presence of green fluorescence within these cells confirmed that exosomes from ectopic endometrial cells were successfully delivered into F11 cells (Fig. 4A). F11 cells were transfected with both a mimic and an inhibitor of miR-92a-3p, and the transfection efficiency was verified by real-time PCR (Fig. 4B). The CCK-8 assay revealed that the upregulation of miR-92a-3p led to an increase in the proliferation rate of F11 cells compared to the negative control (Fig. 4C). Conversely, the downregulation of miR-92a-3p resulted in a decrease in cell proliferation. Furthermore, the Transwell assay demonstrated that miR-92a-3p enhanced the migration and invasion capabilities of F11 cells while its suppression hindered these processes (Fig. 4D). Overall, our results indicated that miR-92a-3p derived from adenomyotic ectopic lesions promotes the proliferation, migration, and infiltration of DRG, which may be related to the pain mechanism of adenomyosis.

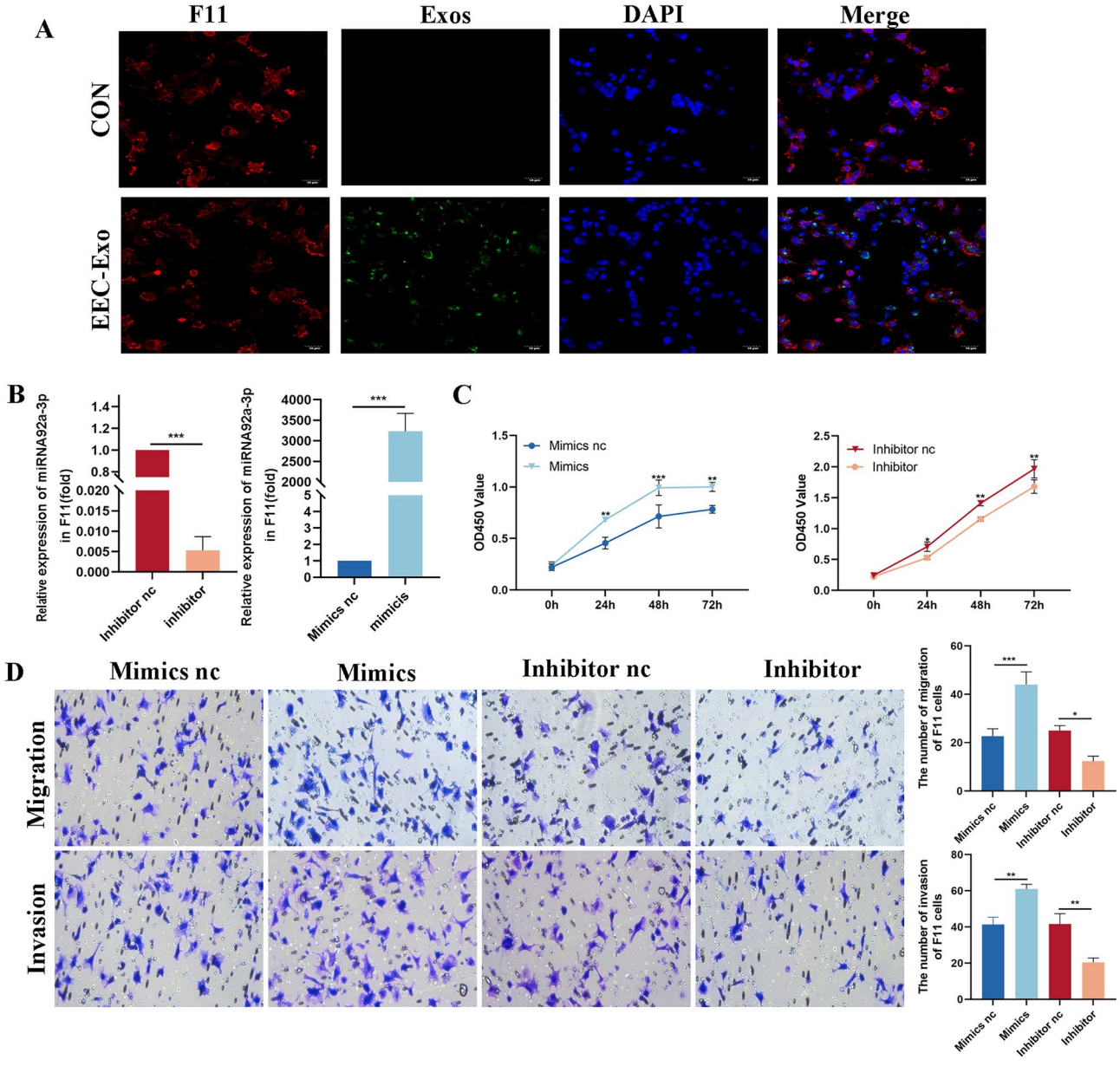

Figure 4. Effects of miR-92a-3p in exosomes derived from ectopic lesions of adenomyosis on the proliferation, migration and invasion of F11. (**A**) The presence of green fluorescence within F11 stained with phalloidine (red). Cell nuclei were stained with DAPI (blue). Scale bars = 50 μm. (**B**) qRT-PCR verified F11 transfection efficiency. (**C**) The CCK8 assay was used to evaluate the proliferation of F11 with transfection. (**D**) Display exemplar images depicting transwell matrigel invasion and migration assays conducted on F11 cells pre-treated with transfection. $^{*}P < 0.05$, $^{**}P < 0.01$ and $^{***}P < 0.001$.

MiR-92a-3p in ELA-exo promotes HUVEC proliferation, migration, infiltration, and tube formation

We observed the effect of miR-92a-3p in exosomes derived from ectopic adenomyotic lesions in HUVECs. Co-culturing of HUVECs with PKH67-labelled exosomes and confocal microscopy showed that exosomes from ectopic endometrial cells were successfully delivered to HUVECs (Fig. 5A). HUVECs were transfected with a mimic or an inhibitor of miR-92a-3p, and the transfection efficiency was confirmed by real-time PCR (Fig. 5B). CCK-8 experiments showed that after the upregulation of miR-92a-3p, HUVECs exhibited a higher proliferation rate compared to the negative control (Fig. 5C), and downregulation of miR-92a-3p inhibited HUVECs proliferation. Transwell assays showed that miR-92a-3p promoted migration and invasion and that downregulation of miR-92a-3p inhibited the migration and invasion of HUVECs (Fig. 5D). Finally, tube formation assay showed that miR-92a-3p promoted HUVECs tube formation, and the downregulation of miR-

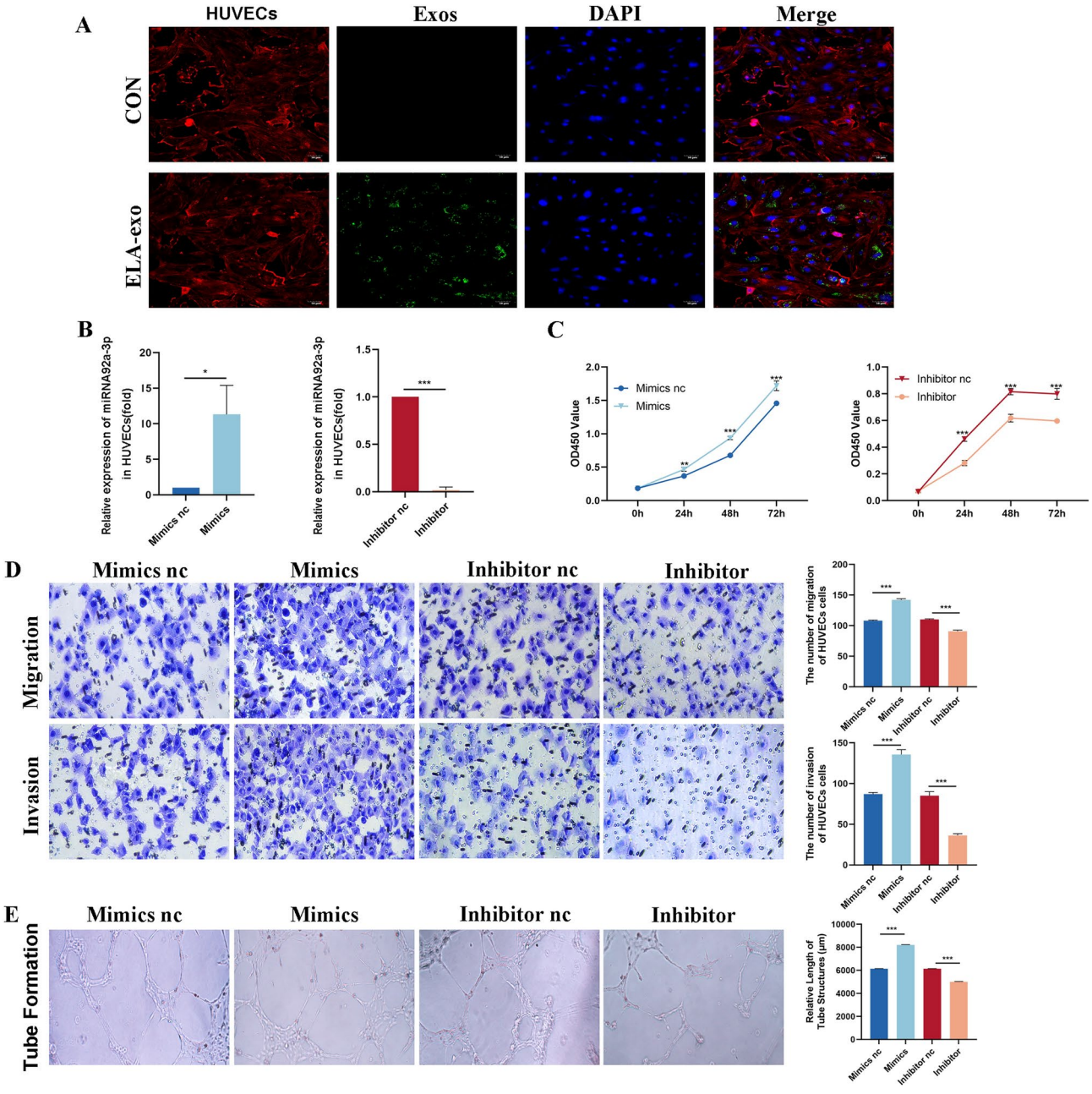

Figure 5. Effects of miR-92a-3p in exosomes derived from ectopic lesions of adenomyosis on the proliferation, migration, invasion and tube formation of HUVECs. (**A**) Confocal images of co-culturing HUVECs with the PKH67-labeled exosomes. Scale bars = 50 μm. (**B**) The efficiency of transfection was confirmed by real-time PCR. (**C**) The CCK8 assay was used to evaluate the proliferation of HUVECs with transfection. (**D**) Transwell assay showed that miR-92a-3p promotes migration and invasion. (**E**) Representative images of miR-92a-3p-mimics -induced tube formation and quantified results. $^{*}P < 0.05$, $^{**}P < 0.01$ and $^{***}P < 0.001$.

92a-3p resulted in reduced tube formation (Fig. 5E). Overall, our results indicate that miR-92a-3p derived from adenomyotic ectopic lesions promoted the proliferation, migration, infiltration, and tube formation of HUVECs, thereby promoting angiogenesis and the progression of adenomyosis.

Expression levels of miR-92a-3p in exosomes relate to clinical symptoms non-invasive detection of miR-92a-3p levels in urinary exosomes has application value in adenomyosis

We analysed the relationship between the expression of miR-92a-3p in exosomes derived from ectopic lesion tissues and the clinical symptoms of patients with adenomyosis. The results showed that the expression level of miR-92a-3p in exosomes was positively correlated with uterine volume in patients with adenomyosis (Fig. 6A). Simultaneously, we found that the expression of miR-92a-3p in exosomes was significantly upregulated in patients with adenomyosis experiencing severe pain and hypermenorrhoea (Fig. 6B,C). However, ectopic lesion tissues cannot be obtained from patients for a clinical diagnosis.

We further attempted to detect the expression levels of miR-92a-3p in exosomes derived from the urine (41 patients with adenomyosis and 16 patients no-adenomyosis controls) (Fig. 6D). The results showed that, compared to the controls, the expression level of miR-92a-3p in the urinary exosomes of patients with adenomyosis was significantly upregulated and correlated with the clinical symptoms of uterine volume, dysmenorrhoea, and menstrual flow (Table 1). This correlation was consistent with the trend observed in the expression levels of miR-92a-3p in exosomes derived from ectopic lesion tissue in adenomyosis (Fig. 6E,F). ROC curve analysis of urinary exosome-derived miR-92a-3p was performed to evaluate its value in adenomyosis. The AUC for urinary exosomal miR-92a-3p was 0.9435 (Fig. 6G). Finally, urine samples were collected from seven patients with adenomyosis before and after radical hysterectomy to compare the expression levels of miR-92a-3p in urine exosomes. The results showed that, compared to before surgery, the level of exosomal miR-92a-3p in urine decreased significantly after surgery (Fig. 6H). This finding provides a strong theoretical basis for the use of urinary exosomal miR-92a-3p as a non-invasive and effective specific biomarker for adenomyosis.

Discussion

Adenomyosis is a chronic and refractory disease[15–17]that often leads to symptoms such as heavy menstrual bleeding, severe dysmenorrhoea, increased uterine size, and infertility[18,19].Despite its prevalence, the pathophysiology of adenomyosis remains poorly understood, hindering its effective diagnosis and treatment. Our study aimed to address this gap by focusing on the role of miR-92a-3p in adenomyosis. We discovered that this miRNA, highly expressed in exosomes derived from ectopic lesions, significantly influences the behaviour of various cell types, including endometrial cells, DRG, and HUVECs. We discovered upregulated miR-92a-3p levels in patient urine-derived exosomes, highlighting its potential as a non-invasive biomarker. This insight provides a deeper understanding of the molecular mechanisms underlying adenomyosis and opens new avenues for non-invasive diagnosis and targeted therapeutic strategies.

Our findings on the role of miR-92a-3p in adenomyosis align with and expand upon existing research in the field of exosomal miRNAs. The elevated expression and impact of miR-92a-3p in adenomyosis offer novel insights, distinct from its known roles in other conditions. A recent study highlighted the role of the exosomal miRNA regulatory network in endometriosis progression, a condition closely related to adenomyosis. Different miRNAs were upregulated, suggesting a unique miRNA profile for each gynaecological condition[20].It has been reported that miR-92a-3p promotes the occurrence and development of tumours in some malignant diseases. Furthermore, Xiao et al. found that the expression of exosomal miR-92a-3p as a biomarker could predict the response to first-line chemotherapy in colorectal cancer, which is consistent with our observations in adenomyosis[21].

This study elucidated a novel exosome-mediated mechanism that promotes migration, nerve cell invasion, and pro-angiogenic endothelial cell behavior, which drives the onset and progression of adenomyosis. The central role of miR-92a-3p highlights its potential as a therapeutic target and biomarker. Further research should explore antagonising miR-92a-3p as a strategy to inhibit cellular infiltration and lesion vascularisation. Detecting elevated miR-92a-3p levels in minimally invasive biofluids might also enable the early diagnosis and monitoring of adenomyosis severity.

By uncovering this exosomal signalling pathway centred on miR-92a-3p, our findings open new possibilities for practical clinical applications. Simple urine tests measuring exosomal miR-92a-3p might provide non-invasive diagnostic screening for adenomyosis. Treatments that block the release or uptake of miR-92a-3p-containing exosomes could offer more targeted control of lesion progression and symptoms than surgery.

Our study has certain limitations. The sample sizes, particularly those of clinical samples, should be expanded in future investigations. We relied extensively on in vitro cell culture models, which do not fully capture in vivo complexity. Although suggestive, our findings relating exosomal miR-92a-3p to symptoms did not prove causality. Future studies are required to validate our conclusions in clinical samples and animal models to strengthen the evidence. From a clinical perspective, large-scale validation of urinary exosomal miR-92a-3p as a non-invasive biomarker is crucial to further strengthen our findings.

Conclusions

This study revealed an exosomal signalling pathway by which adenomyotic lesions promote infiltration and angiogenesis via miR-92a-3p. Our findings identified a promising biomarker and therapeutic target, elucidated early disease mechanisms, and laid the groundwork for the development of improved clinical diagnosis and management of adenomyosis.

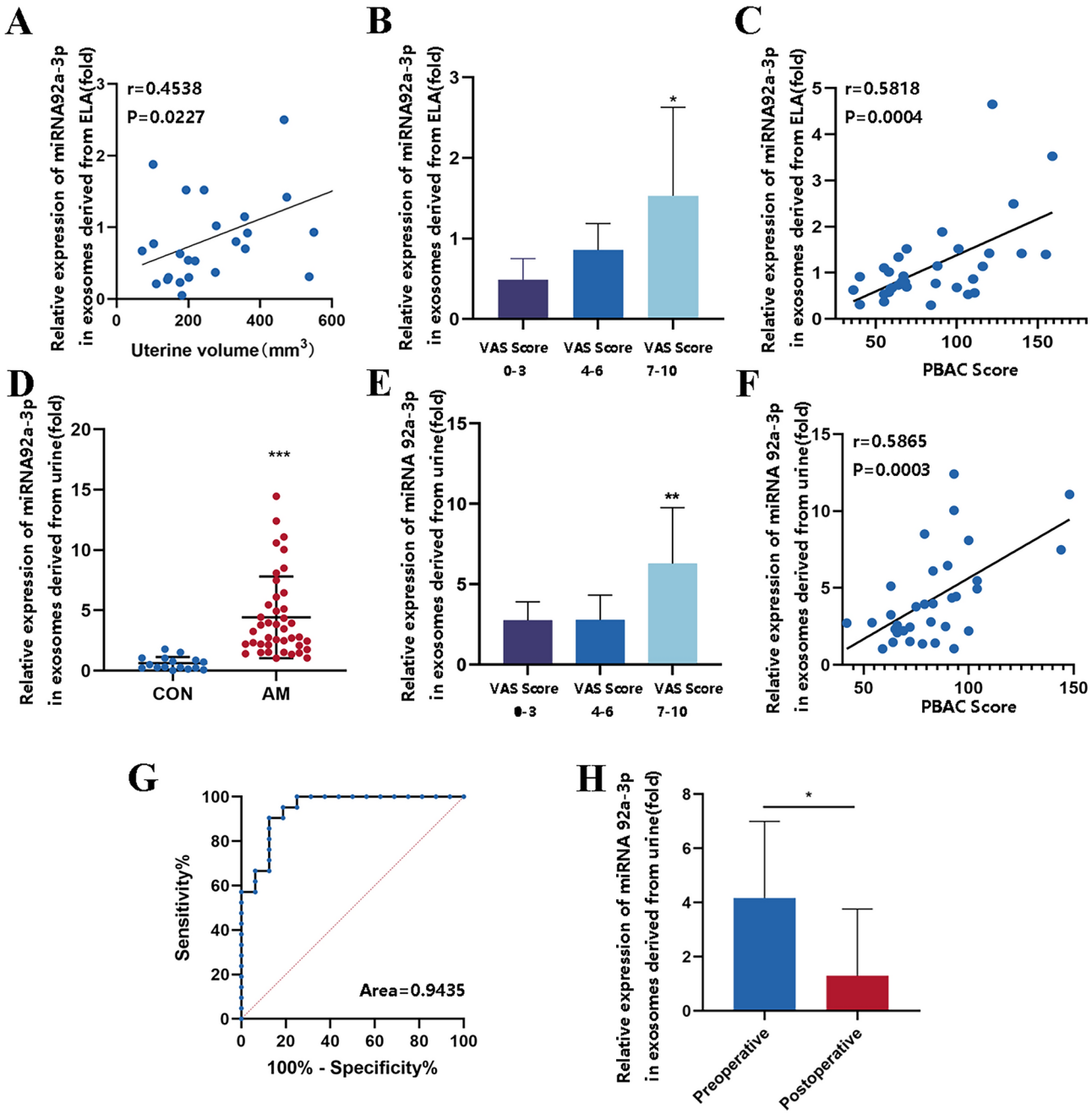

Figure 6. The correlation between the expression of exosome miR-92a-3p and clinical symptoms. (**A**) Pearson correlation analysis between the expression of miR-92a-3p in exosome derived from ectopic lesions of adenomyosis (ELA) and uterine volume in patients with adenomyosis . (**B**) Relationship between the severity of dysmenorrhea and the expression level of miR-92a-3p in exosome derived from ectopic lesions of adenomyosis (ELA). (**C**) Pearson correlation analysis between the expression level of miR-92a-3p in exosome derived from ectopic lesions of adenomyosis (ELA) and menstrual blood volume. (**D**) qRT-PCR was used to detect the expression levels of miR-92a-3p in exosomes derived from the urine. (**E**) Relationship between the severity of dysmenorrhea and the expression level of urinary exosome-derived miR-92a-3p. (**F**) Pearson correlation analysis between the expression level of urinary exosome-derived miR-92a-3p and menstrual blood volume. (**G**) ROC curve analysis of urinary exosome-derived miR-92a-3p in diagnosis of adenomyosis. (**H**) Comparison of preoperative and postoperative miR-92a-3p expression levels in patients with high expression of urinary exosomal miR-92a-3p. The severity of dysmenorrhea is assessed by visual analogue scale (VAS). Menstrual blood volume is assessed using Pictorial Blood Loss Assessment Chart (PBAC).

Variable	Adenomyosis	Control	*P* value
Age	47.27 ± 3.17	47.54 ± 4.37	0.98
Abortion	2 ± 1.41	1.92 ± 1.5	0.92
Parity	1.47 ± 1.01	1.31 ± 0.48	0.79
Uterine volume	155.06 ± 177	229.12 ± 128.33	0.05
VAS	5.27 ± 3.02	0.69 ± 1.49	< 0.001
PBAC	88.27 ± 28.07	45.08 ± 17.76	< 0.001
Ca-125	140.24 ± 154.76	15.04 ± 6.52	< 0.001
Hemoglobin	103.24 ± 21.27	119.38 ± 14.45	0.06
Gravidity	3.47 ± 1.66	3.23 ± 1.64	0.97

Table 1. Association of miR-92a-3p in urinary exosomes expression with the clinicopathological characteristics of adenomyosis patients. Data are expressed as mean ± standard deviation. Uterine volume was assessed using the formula for an ovoid (length × width × depth × 0.52). VAS: VAS was used to evaluate the intensity of adenomyosis-associated dysmenorrhea. Score ranged from 0 to 10, and a higher score represented a greater intensity of pain. PBAC: The menstrual blood loss was analyzed with the Pictorial Blood Loss Assessment Chart

Data availability

The datasets generated and analysed during the current study are available in the NCBI Gene Expression Omnibus with the primary accession code PRJNA1091186, https://www.ncbi.nlm.nih.gov/geo/query/acc.cgi?acc=GSE262302

Received: 16 February 2024; Accepted: 24 December 2024
Published online: 22 March 2025

References

1. Vercellini, P. et al. Association of endometriosis and adenomyosis with pregnancy and infertility. *Fertil. Steril.* **119**(5), 727–740 (2023).
2. Yildiz, S. et al. Adenomyosis: Single-cell transcriptomic analysis reveals a paracrine mesenchymal-epithelial interaction involving the wnt/sfrp pathway. *Fertil. Steril.* **119**, 869–882 (2023).
3. Jiang, X. & Chen, X. Endometrial cell-derived exosomes facilitate the development of adenomyosis via the il-6/jak2/stat3 pathway. *Exp. Ther. Med.* **26**, 1–8 (2023).
4. Juárez-Barber, E. et al. Extracellular vesicles secreted by adenomyosis endometrial organoids contain miRNAs involved in embryo implantation and pregnancy. *Reprod. BioMed. Online* **46**, 470–481 (2023).
5. Guo, Z. et al. RNA-seq reveals co-dysregulated circular RNAs in the adenomyosis eutopic endometrium and endometrial-myometrial interface. *BMC Women's Health* **22**, 293 (2022).
6. Brubel, R. et al. Serum galectin-9 as a noninvasive biomarker for the detection of endometriosis and pelvic pain or infertility-related gynecologic disorders. *Fertil. Steril.* **108**, 1016–1025 (2017).
7. Cho, S., Mutlu, L., Grechukhina, O. & Taylor, H. S. Circulating micrornas as potential biomarkers for endometriosis. *Fertil. Steril.* **103**, 1252–1260 (2015).
8. Mao, Q. et al. miR-92a-3p promotes the proliferation and invasion of gastric cancer cells by targeting klf2. *J. Biol. Regul. Homeost. Agents* **34**, 1333–1341 (2020).
9. Jinghua, H. et al. Microrna miR-92a-3p regulates breast cancer cell proliferation and metastasis via regulating b-cell translocation gene 2 (btg2). *Bioengineered* **12**, 2033–2044 (2021).
10. Ashok, G., Das, R., Anbarasu, A. & Ramaiah, S. Comprehensive analysis on the diagnostic role of circulatory exosome-based miR-92a-3p for osteoblastic metastases in prostate adenocarcinoma. *J. Mol. Recognit.* **36**, e3042 (2023).
11. Li, J.-L. & Luo, P. Mir-140-5p and miR-92a-3p suppress the cell proliferation, migration and invasion and promoted apoptosis in Wilms' tumor by targeting frs2. *Eur. Rev. Med. Pharmacol. Sci.* **24**, 97–108 (2020).
12. Zhang, L. et al. Serum exosomal micrornas as potential circulating biomarkers for endometriosis. *Dis. Mark* **2020**, 2456340 (2020).
13. Chen, J. et al. Review on strategies and technologies for exosome isolation and purification. *Front. Bioeng. Biotechnol.* **9**, 811971 (2022).
14. Théry, C., Amigorena, S., Raposo, G. & Clayton, A. Isolation and characterization of exosomes from cell culture supernatants and biological fluids. *Curr. Protoc. Cell Biol.* **30**, 3–22 (2006).
15. Zhai, J., Vannuccini, S., Petraglia, F. & Giudice, L. C. Adenomyosis: Mechanisms and pathogenesis. in *Seminars in Reproductive Medicine*, vol. 38, 129–143 (Thieme Medical Publishers, Inc. 333 Seventh Avenue, 18th Floor, 2020).
16. Moldassarina, R. S. Modern view on the diagnostics and treatment of adenomyosis. *Arch. Gynecol. Obstet.* 1–11 (2023).
17. Chen, J., Porter, A. E. & Kho, K. A. Current and future surgical and interventional management options for adenomyosis. in *Seminars in Reproductive Medicine*, vol. 38, 157–167 (Thieme Medical Publishers, Inc. 333 Seventh Avenue, 18th Floor, 2020).
18. Schrager, S., Yogendran, L., Marquez, C. M. & Sadowski, E. A. Adenomyosis: Diagnosis and management. *Am. Fam. Phys.* **105**, 33–38 (2022).
19. Yang, B. et al. Immunoreactivity of plasminogen activator inhibitor 1 and its correlation with dysmenorrhea and lesional fibrosis in adenomyosis. *Reprod. Sci.* **28**, 2378–2386 (2021).
20. Wu, J. et al. Construction and topological analysis of an endometriosis-related exosomal circRNA–miRNA–mRNA regulatory network. *Aging (Albany NY)* **13**, 12607 (2021).
21. Gherman, A. et al. Baseline expression of exosomal miR-92a-3p and mir-221-3p could predict the response to first-line chemotherapy and survival in metastatic colorectal cancer. *Int. J. Mol. Sci.* **24**, 10622 (2023).

Acknowledgements

We thank the patients and negative volunteers for their participation.

Author contributions

Conceptualization, W.S. and Y.Y.; methodology, W.S., Y.Y. and J.W.; software, W.S.; validation, W.S., Y.Y. and J.W.; formal analysis, W.S., Y.Y. and X.C.; investigation, W.S., X.C. and X.L.; resources, W.S., X.C., Y.C. and W.Z; data curation, Z.Q., S.M. and T.C.; writing-original draft preparation, W.S.; writing-review and editing, W.S., Y.Y. and J.W.; visualization, Y.Y.; supervision, X.C.; project administration, X.C. and X.L.; funding acquisition, X.C. All authors have read and agreed to the published version of the manuscript.

Declarations

Competing interests

No conflicts of interest, financial or otherwise, are declared by the authors.

Additional information

Supplementary Information The online version contains supplementary material available at https://doi.org/10.1038/s41598-024-84608-5.

Correspondence and requests for materials should be addressed to X.L. or X.C.

Reprints and permissions information is available at www.nature.com/reprints.

Publisher's note Springer Nature remains neutral with regard to jurisdictional claims in published maps and institutional affiliations.